Journal of Pharmaceutical and Biomedical Analysis 219 (2022) 114860

Contents lists available at ScienceDirect

Journal of Pharmaceutical and Biomedical Analysis

journal homepage: www.journals.elsevier.com/journal-of-pharmaceutical-and-biomedical-analysis

Novel plasma protein binding analysis method for a PET tracer and its radiometabolites: A case study with [^{11}C]SMW139 to explain the high uptake of radiometabolites in mouse brain

Richard Aarnio [a,b,c], Obada M. Alzghool [a,b], Saara Wahlroos [c], James O'Brien-Brown [d], Michael Kassiou [d], Olof Solin [c,e,f], Juha O. Rinne [c,g], Sarita Forsback [c], Merja Haaparanta-Solin [a,*]

[a] MediCity Research Laboratory, University of Turku, Tykistökatu 6A, FI-20520 Turku, Finland
[b] Drug Research Doctoral Programme, University of Turku, Turku, Finland
[c] Turku PET Centre, University of Turku, Kiinamyllynkatu 4-8, FI-20520 Turku, Finland
[d] School of Chemistry, The University of Sydney, Sydney, NSW 2006, Australia
[e] Department of Chemistry, University of Turku, Henrikinkatu 2, FI-20500 Turku, Finland
[f] Accelerator Laboratory, Turku PET Centre, Åbo Akademi University, Kiinamyllynkatu 4-8, FI-20520 Turku, Finland
[g] Division of Clinical Neurosciences, Turku University Hospital, Turku, Finland

ARTICLE INFO

Keywords:
Plasma protein binding
Ultrafiltration
RadioTLC
[^{11}C]SMW139
Radiometabolite analysis
Parent fraction
Positron emission tomography

ABSTRACT

Radiometabolites of PET tracers interfere with imaging and need to be taken into account when modeling PET data. Various tracer and radiometabolite characteristics affect the uptake rate into tissue. In this study, we investigated two such factors, lipophilicity and protein-free fraction. A novel rapid method was developed using thin-layer chromatography with digital autoradiography (radioTLC) and ultrafiltration for analyzing the protein-free fractions of an exemplar PET tracer, [^{11}C]SMW139 (f_P, free parent tracer over all radioactivity), and its radiometabolites (f_M, free radiometabolites over all radioactivity). Detailed understanding of the uptake of radiometabolites into extravascular cells requires analyzing f_M, which has not previously been performed for PET tracers. Mice were injected with [^{11}C]SMW139, and time-activity curves from plasma and brain coupled with the parent fraction and free fraction data were analyzed to demonstrate the true levels of protein-free and protein-bound [^{11}C]SMW139 and its radiometabolites in plasma. The ultrafiltration method included separate membrane correction factors for the parent tracer and its radiometabolites for analysis of unbiased f_P and f_M. Metabolism of [^{11}C]SMW139 was rapid, and after 45 min, the parent fraction was 0.33 in plasma and 0.28 in brain. Ultrafiltration membrane correction had a significant effect on the f_P but not the f_M. From 10–45 min, the f_P decreased from 0.032 to 0.007, while f_M remained between 0.52 and 0.35. The much higher f_M in plasma could explain why the less lipophilic radiometabolites enter the brain efficiently. This detailed understanding of f_P and f_M from rodents can be used in translational studies to explain the behavior of the tracer in humans. Similar parent fraction and plasma protein binding methods can be used for human *in vivo* analysis.

1. Introduction

Positron emission tomography (PET) is a medical imaging technique for the quantitative measurement of metabolic processes *in vivo* by means of a PET tracer. Neuroimaging is one field where the non-invasiveness of PET is valuable. For intravenous use in neuroimaging, the PET tracer needs to have specific characteristics, including the ability to cross the blood–brain barrier (BBB) and bind with high specificity to the desired target in the brain [1]. The pharmacokinetics of the tracer must be well understood for PET data to be interpreted correctly. Therefore, in this study, we aimed to develop methods to study some of the key properties of tracers and to explain what underlies their distribution, metabolism, and excretion characteristics.

An analyte's lipophilicity, for example, is an important determinant of its ability to cross the BBB. The increased lipophilicity affects the crossing of the BBB by two mechanisms: aiding it by improving the solubility into the lipid bilayer of the endothelial cell membrane [2] and by hampering it by increasing the protein-bound fraction. A previous

* Correspondence to: Turku PET Centre, University of Turku, Tykistökatu 6A, 4th floor, FI-20520 Turku, Finland.
E-mail address: mehaaso@utu.fi (M. Haaparanta-Solin).

https://doi.org/10.1016/j.jpba.2022.114860
Received 9 December 2021; Received in revised form 20 May 2022; Accepted 25 May 2022
Available online 28 May 2022

study by Zoghbi et al. has shown the correlation between the lipophilicity of tracers and the parent free fraction (*i.e.*, free parent tracer over all radioactivity in plasma, f_P), indicating that the high lipophilicity correlates with low f_P [3]. However, how the body metabolizes the parent tracer generally reduces its lipophilicity, as in glucuronidation, which aids renal excretion but yields metabolites with increased hydrophilicity and lower BBB-penetrating abilities. Also, to effectively cross the BBB, the analyte must be free, *i.e.*, not bound to proteins in the vascular system [1,4,5], making studies of the free fraction crucial for determining the true input of the parent tracer and its radiometabolites. Other tracer characteristics also affect BBB penetration, but here we focused on the protein-free fraction and lipophilicity characteristics.

The uptake of radiometabolites in the target organ often disturbs the analysis of the uptake and specific binding of the original PET tracer, hampering analysis of the PET data. PET detects the signal originating from the annihilation of any positron, so it cannot distinguish whether the signal originates from the parent tracer or its radiometabolites. For this reason, investigating the radiometabolism of tracers reveals the true parent concentration in the target organ. Combining this information with knowledge of the tracer protein binding and its radiometabolites can yield the correct input to extravascular tissue during a PET study.

To our knowledge, the plasma protein binding of radiometabolites has not been previously analyzed separately from the parent tracer. Robust and rapid methods to separate the protein-free and protein-bound parent tracer and radiometabolites from each other need to be developed to quantify the f_P and separately the free fraction of radiometabolites in plasma (free radiometabolites over all radioactivity in plasma, f_M). The novel method introduced here combines a new rapid and robust radiometabolite analysis method using thin-layer chromatography combined with digital autoradiography (radioTLC) for parent fraction analysis and an ultrafiltration (UF) method to analyze the f_P and f_M. In addition, filter membrane correction factors are determined separately for parent tracer and its radiometabolites that take into account the various sources of error, such as nonspecific binding to the UF device and different mobilities through the semipermeable membrane of plasma water and analytes from the same plasma matrix. These factors are commonly acknowledged sources of error in a UF method and various ways to overcome these effects have been introduced [6,7]. However, the applied correction methods (*i.e.*, pretreatment) to minimize nonspecific binding often may introduce other error sources. Many other methods to analyze the f_P have been developed [8]. Further development and comparison of these methods is important for standardization and to make best practices widely available.

The $P2X_7$ receptor antagonist 2-chloro-5-[^{11}C]methoxy-N-((3,5,7-trifluoroadamantan-1-yl)methyl)benzamide ([^{11}C]SMW139) (Fig. 1) is a novel tracer for imaging the $P2X_7$ receptor [9,10]. In the brain, $P2X_7$ receptor is predominantly expressed in microglia and is involved in mediating neuroinflammation [11,12]. Hence, [^{11}C]SMW139 holds broad potential for use in detecting and quantitating neuroinflammation in several neurodegenerative conditions, including Alzheimer's disease, Parkinson's disease, and multiple sclerosis [13,14]. The first radiometabolite study of [^{11}C]SMW139 used a high-performance liquid chromatography system combined with a radiodetector (radioHPLC) method to analyze the parent fraction in rat plasma and brain tissue [9]. Janssen et al. have shown that radiometabolites of [^{11}C]SMW139 are found in large concentrations in rat brain tissue even though less lipophilic radiometabolites in general have worse BBB-penetrating abilities compared to the more lipophilic parent tracer, raising the question of why they enter the brain so effectively. Answering this question requires studying the free fractions in more detail.

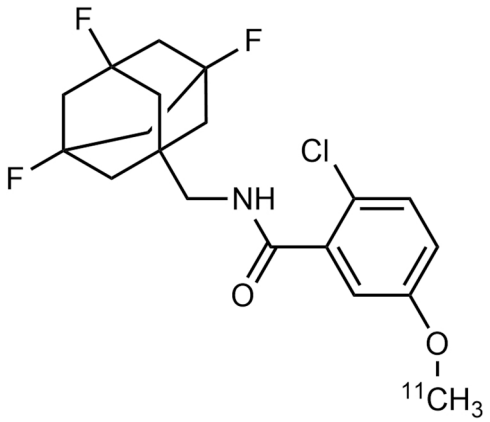

Fig. 1. Chemical structure of [^{11}C]SMW139.

In this study, *in vitro* mouse brain homogenate studies were performed to address whether the radiometabolites actually penetrate the BBB or are formed in the brain after penetration of the parent tracer. In addition, time-activity curves (TACs) of plasma and brain were analyzed from a large number of mice injected with [^{11}C]SMW139 to demonstrate the difference in the free fraction–corrected concentrations of the parent tracer and its radiometabolites.

Here, we introduce a novel method to determine the f_P of the parent tracer [^{11}C]SMW139 and f_M in mouse plasma. This work adds a more detailed understanding of the pharmacokinetic properties and aids in modeling the uptake of [^{11}C]SMW139 into organs. By studying the f_M and comparing it with the f_P, we can also partly explain why a less lipophilic tracer enters the brain so efficiently.

2. Material and methods

2.1. Radiochemistry

[^{11}C]SMW139 was synthesized at the Radiopharmaceutical Chemistry Laboratory of Turku PET Centre (for the synthesis procedure, see supplementary materials). A total of 27 syntheses were used for the animals in this study. At the end of synthesis, the radiochemical purity was 98.3 ± 0.5 %, and the molar activity was 110 ± 49 GBq/μmol. All work with radioactivity was performed following the regulations from the Finnish Radiation and Nuclear Safety Authority.

2.2. Experimental animals and chemicals

This study was performed in accordance with the EU Directive 2010/63/EU on the protection of animals used for scientific purposes, and in keeping with the ARRIVE guidelines. All animal procedures were approved by the Regional State Administrative Agency for Southern Finland (license number ESAVI/16273/2019).

Three to four mice were group-housed in individually ventilated cages with the following standard conditions: temperature 21 ± 1.2 °C, humidity 55 % ± 5 %, and a 12-h light/dark cycle. Soy-free chow (RM3 (E) Soya Free, 801710, Special Diets Service, Essex, UK) and tap water were provided *ad libitum*.

For this study, 73 C57BL/6 J (43 females and 30 males; 31.7 ± 5.5 g) mice were bred and maintained according to the guidelines of the International Council of Laboratory Animal Science (ICLAS) in the Central Animal Laboratory of University of Turku. Animal studies were performed in accordance with the European Ethics Committee (decree 86/609/CEE). The mice were injected with [^{11}C]SMW139 (14.5 ± 5.8 MBq; molar activity at the time of injection, 37 ± 27 GBq/μmol; injected mass per body weight, 8.3 ± 6.9 μg/kg). All of the chemicals for the preclinical experiments were HPLC-grade and obtained from Sigma-Aldrich.

2.3. Collection of mouse plasma and brain samples and radioactivity measurements

Blood samples (200–500 μL) were collected under deep isoflurane anesthesia by cardiac puncture into heparinized gel tubes (Microtainer,

Becton, Dickinson and Company, Franklin Lakes, NJ). Transcardial perfusion with saline was conducted to eliminate the blood from the brain. The blood was centrifuged (12,100 ×*g*, 90 s) to separate the plasma so that the TAC of plasma could be determined as percentage of injected radioactivity per gram of tissue (%IA/g) at 10-min (n = 45), 30-min (n = 14), and 45-min (n = 7) time points post radiotracer injection (p.i.). This step was accomplished by using a cross-calibrated automated gamma counter (Wizard^2 2480 3", PerkinElmer, Turku, Finland) to measure the decay-corrected radioactivity of the plasma and brain.

2.4. Parent fraction analysis of plasma and brain samples

For chromatographic analyses, the plasma was pipetted into an Eppendorf tube and mixed with acetonitrile (plasma:acetonitrile 1:2 *v/v*) to precipitate the plasma proteins. The mixture was vortexed for approximately 10 s and centrifuged (12,100 × *g*, 90 s), and the supernatant was collected for radioTLC analysis.

The brain tissue was cut into pieces, and approximately one third of the brain was homogenized into the TLC mobile phase. The homogenate was centrifuged (12,100 × *g*, 90 s), and the clear supernatant was used for TLC analysis.

Various radioTLC methods were tested to find a fast and robust separation of the parent tracer and its radiometabolites and the following method parameter goals were used to guide the method selection process: a retardation factor (R_f) of 0.3–0.5 for the parent tracer with more polar radiometabolites eluting with R_f 0.6–0.9 was deemed optimal. A baseline separation with resolution above 1.5 was required between the parent tracer and its radiometabolites. In addition, efforts were made to optimize the separation of different radiometabolites, but separation of the parent tracer from all of the other radioactive components in the sample was prioritized. The following TLC-plate and TLC mobile phase combinations were tested: high-performance TLC (HPTLC, silica gel 60 RP-18, art no. 1.05914.0001, Merck KGaA, Darmstadt, Germany), TLC (Silica gel 60 RP-18. art no. 1.05559.0001, Merck KGaA), and HPTLC W (W = wettable, silica gel 60 RP-18 W, art no. 1.14296.0001, Merck KGaA) plates were examined with various acetonitrile, water, and trifluoroacetic acid compositions ranging from 60 % to 75 % organic and 0.1–0.4 % acid modifier compositions. The gas phase was allowed to saturate (>45 min) before the elution chamber was used (10 × 10 cm Twin Trough Chamber, Camag, Muttenz, Switzerland; volume of mobile phase: 15 mL).

The best method for a fast and robust separation of the parent tracer from its radiometabolites was selected and is described below. A [^{11}C]SMW139 standard (30 Bq/μL) was prepared in the TLC mobile phase. Standard (5 μL), plasma (10 μL), and brain (10 μL) supernatants (Fig. 2) were applied with a pipette onto the TLC plate (Silica gel 60 RP-18, art no. 1.05559.0001, Merck KGaA) and acetonitrile:water:trifluoroacetic acid (65:35:0:1 *v/v/v*) was used as the TLC mobile phase. The TLC plate was developed until the migration distance was 4 cm. Additional samples were applied to this same plate, as described in Section 2.6. The developed and dried plate was exposed to an erased autoradiography imaging plate (BAS-TR2025, Fuji Photo Film Co., Ltd., Tokyo, Japan) for approximately one hour to record the distribution of the separated radioactive compounds. The imaging plate then was scanned with a laser using a BAS-5000 phosphorimager (Fuji Photo Film Co., Ltd., Tokyo, Japan) and analyzed using an Aida Image Analyzer (v.4.22, Elysia-Raytest, GmbH, Straubenhardt, Germany). From the obtained chromatogram, the parent fraction was analyzed as the photostimulated luminescence (PSL) corresponding to the unchanged [^{11}C]SMW139 divided by the total PSL corresponding to the whole sample. Background radioactivity correction was performed on all autoradiography analyses.

The parent fraction was successfully analyzed with the selected method from the following numbers of mice: plasma, 10 min, n = 19; 30 min, n = 14; 45 min, n = 13; and brain: 10 min, n = 9; 30 min, n = 14; 45 min, n = 11.

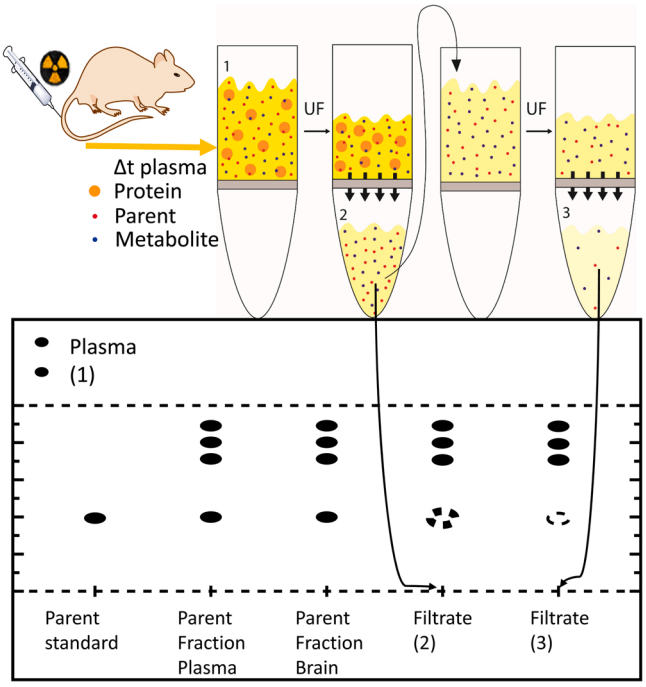

Fig. 2. Depicted design of plasma filtration procedures and [^{11}C]SMW139 standard, plasma, brain, and filtrate (1-3) sample application to TLC plate application line and simulation of the separation of the components in the sample in an autoradiograph of the developed TLC. Application line (lower) and solvent front line (upper) marked with dashed lines. Results are used to calculate the parent fraction in plasma and brain, and to calculate separately the parent and radiometabolite free fraction (f_P and f_M) and filter membrane correction factors.

2.5. Metabolite correlation in plasma and brain

To investigate the correlation between percentage of radiometabolites in plasma and brain, we plotted the percentages of radiometabolites over all radioactivity in plasma and brain from mice with successful parent fraction data for both (n = 47, including data from other tested radioTLC methods (*i.e.*, HPTLC-plate, not only the selected radioTLC method)). The slope, Pearson's correlation (r), and coefficient of determination (R^2) were calculated.

2.6. f_P and f_M in plasma and UF membrane correction

To determine the f_P and f_M, the radioactivity concentration of the *in vivo* plasma sample (c_{plasma}) was measured by applying a known volume of plasma(1) (3 μL) in duplicate on the top part of a TLC plate (Silica gel 60 RP-18, art no. 1.05559.0001, Merck KGaA) above the mobile phase front line (Fig. 2). Autoradiography was used to calculate the PSL/volume concentration. The plasma parent fraction analysis result was used to determine the concentrations of parent tracer (Eq. 1) and its radiometabolites (Eq. 2) in the plasma sample as follows:

$$c_{\text{plasma,parent}} = \text{parent } \textit{fraction} * c_{plasma} \quad (1)$$

$$c_{\text{plasma,metabolites}} = (1 - \text{parent fraction}) * c_{plasma} \quad (2)$$

To separate the protein-free [^{11}C]SMW139 and its protein-free radiometabolites from the protein-bound ones, we used a 10-kDa UF semipermeable membrane (Microcon-10 kDa Centrifugal Filter Unit with Ultracel-10 membrane, Merck KGaA). Roughly, a minimum of 80 μL of plasma was needed to carry out this analysis, including the membrane correction analysis. The plasma(1) was centrifuged (14,100 ×*g*, 7 min) to gain at least 40 μL of filtrate(2). The filtrate(2) was transferred into another identical UF device and centrifuged for

4 min to gain at least 15 μL of filtrate(3), while the original plasma(1) was simultaneously centrifuged further to collect more of the filtrate(2). A radioactive standard of the parent tracer, a plasma and a brain supernatant sample (as described in Section 2.4), filtrate(2) (10 μL), and filtrate(3) (10 μL) were applied onto the application line of the same TLC plate (Fig. 2). The dried plate was developed, digitized, and analyzed as described in Section 2.4.

To calculate the membrane correction factor for the parent tracer, the concentration (PSL/applied volume of sample) ratio of the parent tracer in filtrate(3) and filtrate(2) was calculated as follows:

$$Membrane\quad correction_{\text{parent}} = \frac{c_{parent\quad in\quad filtrate(3)}}{c_{parent\quad in\quad filtrate(2)}} \tag{7}$$

The parent concentration in filtrate(2) was divided by the membrane

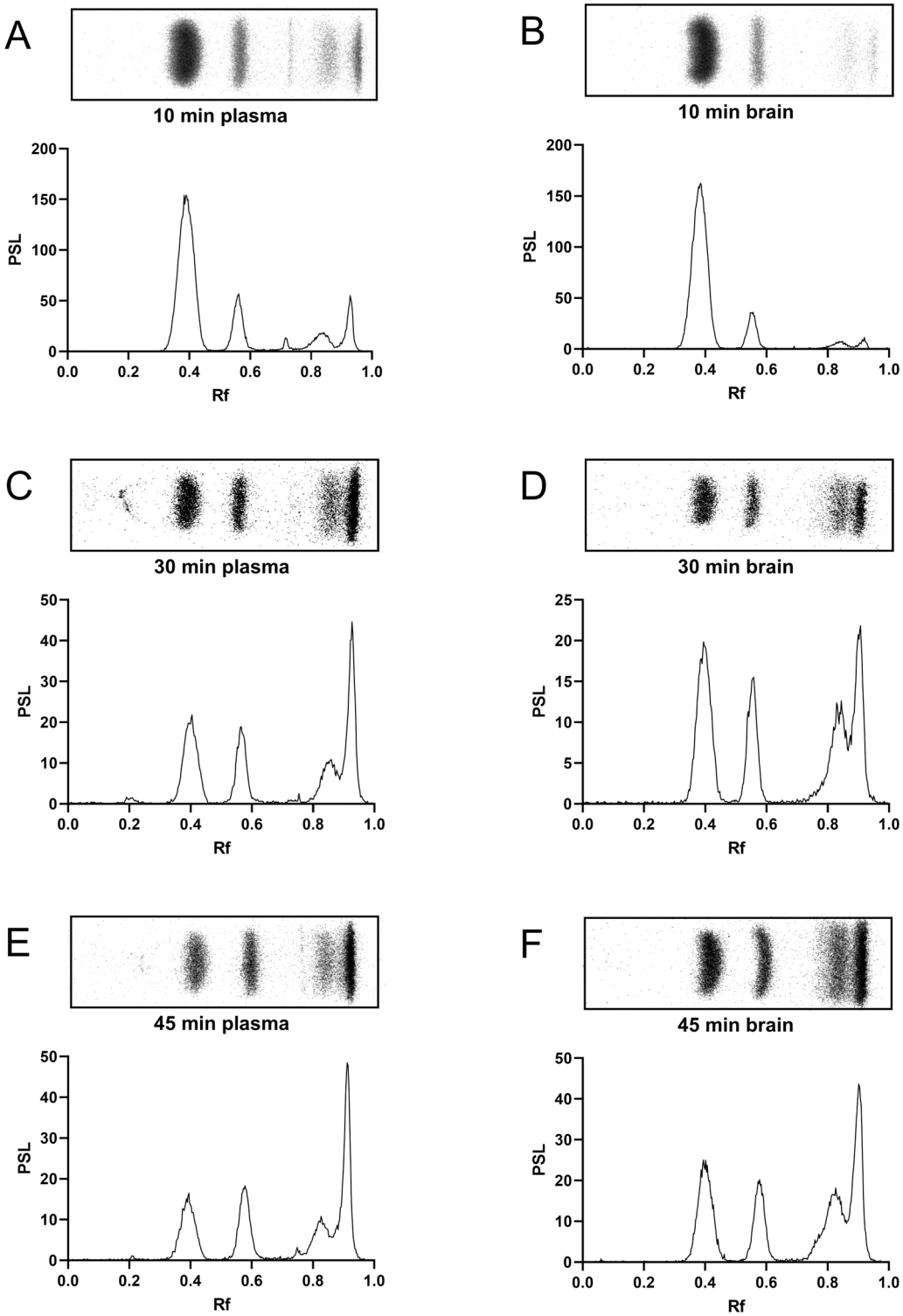

Fig. 3. Representative digital autoradiograph images and corresponding chromatograms of parent tracer and its radiometabolites for different time points. (A) 10 min plasma, (B) 10 min brain, (C) 30 min plasma, (D) 30 min brain, (E) 45 min plasma, and (F) 45 min brain. Standard sample confirmed that the R_f for the parent tracer is 0.4.

correction factor to calculate the true amount of the free parent in the filtrate(2) (as if the membrane would not have limited the amount of free parent passing through the membrane). The corrected free parent concentration in filtrate(2) was divided by the concentration of total radioactivity in plasma(1) to gain f_P. For the radiometabolites, the membrane correction factor and concentration in filtrate(2) was calculated likewise using the values for radiometabolites. The corrected, true concentration of radiometabolites in filtrate(2) was divided by the concentration of all radioactivity in plasma(1) to yield f_M.

2.7. In vitro mouse brain homogenate study

To determine whether radiometabolites can form directly in mouse brain *in vitro*, one mouse was euthanized under deep isoflurane anesthesia by cardiac puncture immediately followed by transcardial perfusion with saline. The freshly dissected mouse brain was homogenized (Ultra-Turrax T8, IKA, Staufen, Germany) in PBS solution (36 °C, 4 mL). A high radioactivity concentration was achieved by adding 1 MBq of [^{11}C]SMW139 to the mixture, followed by vortexing for 1 min at medium speed and then incubation (36 °C, 45 min). The mixture was shaken gently every 5 min. A sample of the incubated brain homogenate was taken at 10, 30, and 45 min. The samples were prepared and analyzed with radioTLC as described in Section 2.4. A sham sample without the brain homogenate was prepared and analyzed exactly as the brain sample with [^{11}C]SMW139. If radiometabolites were found to form in brain tissue *in vitro*, they were analyzed as a fraction of the total radioactivity of the sample.

2.8. Statistics

All results are reported as mean ± standard deviation (SD) where standard deviation could be calculated. The correlation (Section 3.4) was fitted with a simple linear regression, and the slope, r, and R^2 values were analyzed (GraphPad Prism 9, GraphPad Software, San Diego, CA).

3. Results and discussion

3.1. Method selection for analysis of [^{11}C]SMW139 and its radiometabolites

The selected radioTLC method fulfilled all of the requirements for a method with a short run time and high separation power. The mobile phase migration of 4 cm took only 6 min. The method exceeded the required resolution. In addition to separating the parent tracer from all of its radiometabolites, in most cases, the method managed to separate between two to four radiometabolites from each other with almost baseline separation (Fig. 3). Separating the radiometabolites from each other enables more comprehensive modeling if multiple radiometabolite compartments are needed.

Using radioTLC allows for simultaneous analysis of multiple samples with the benefit that samples analyzed on the same autoradiography imaging plate do not need to be decay corrected if only ratios are calculated. This approach is unlike radioHPLC, which involves relatively long run times and the need to run each sample separately, hindering sample throughput and effective use of expensive tracer batches when tracers are labeled with a short-lived radionuclide, such as carbon-11 ($T_{½}$ = 20.4 min). In addition, radioHPLC requires expensive equipment, more solvents, and individual decay correction of all peaks. On the other hand, radioHPLC has some advantages, including more versatile separation options because of, for example, gradient methods. A low radioactivity concentration and low volume samples necessitate extremely sensitive and linear-ranged radioactivity-detecting capabilities. These issues are not associated with the radioTLC method because quantitation of the radioactivity using digital autoradiography for the low radioactivity concentration samples is linear with a wide range of radioactivity [15].

For plasma sample preparation using protein precipitation, we chose the 1:2 ratio of plasma to acetonitrile to effectively precipitate as much as possible of plasma proteins without diluting the sample excessively so that the radioactivity concentration stayed as high as possible for optimal parent fraction quantification. Polson et al. demonstrated that this ratio of plasma and acetonitrile precipitates 96.4 % of the dissolved proteins [16]. Precipitation is intended to enable optimal chromatographic separation by reducing the matrix to prevent TLC plate overload. This effect facilitates absorption of the sample into the TLC plate before elution, as generally C-18–modified TLC plates do not absorb aqueous samples well. In addition, changing the conformation of the proteins with an organic solvent releases the binding between the analytes and proteins [16]. The addition of acetonitrile also increases the solubility of lipophilic analytes into the supernatant instead of their binding to the protein pellet. These effects maximize the radioactivity concentration in the supernatant by increasing the extraction efficiency, which aids parent fraction analysis by enhancing the signal-to-noise ratio and by including all components present in plasma to the analysis. This disruption is especially important as not only the f_P and f_M represent the true parent fraction value in plasma because the compounds also are largely bound to plasma proteins in different ratios and also that part needs to be included in the analysis. The extraction efficiency, *i.e.*, the percentage of radioactivity transferred to the supernatant from the plasma sample for the selected precipitation method was over 99 % for mouse plasma (n = 3). The residual radioactivity of the supernatant was taken into account and deducted from the protein pellet radioactivity.

3.2. TAC and parent fraction in plasma and brain

In this study, the radiometabolite analysis and total and metabolite-corrected TACs of plasma and brain showed that [^{11}C]SMW139 and its radiometabolites cross the BBB and enter the brain (Fig. 4), as previously reported [9]. From 10–45 min p.i., the volume of distribution of the brain (metabolite-corrected radioactivity of brain over metabolite-corrected radioactivity of plasma) decreased slightly from 0.79 to 0.58. The equilibrium value of the volume of distribution was set by 30 min. The metabolite-corrected TACs (Fig. 4) showed a rather steady washout in plasma and brain. A rapid uptake into the target tissue and a steady washout are generally good receptor- or transporter-binding radiotracer characteristics.

The average radiochemical purity of [^{11}C]SMW139 was used as the maximum parent fraction value (0.98). The parent fraction decreased from 0.71 to 0.33 in plasma and from 0.79 to 0.28 in the brain at 10 and 45 min p.i., respectively (Fig. 4). This decrease was more rapid than that seen in humans (data not shown), but the results are similar to those using other separation methods in rats [9].

3.3. Parent and metabolite free fraction in plasma (f_P and f_M)

3.3.1. Membrane correction

To gain unbiased free fraction data, we determined membrane correction values for the Microcon Ultracel UF device individually for the parent tracer and its radiometabolites to calculate the concentration of free parent tracer and radiometabolites in the plasma sample. The membrane correction value for the radiometabolites was 0.93 ± 0.04 (n = 9), indicating that the free radiometabolites passed through the filter membrane with almost no reduction in concentration. However, the concentration of the free parent tracer after filtration was reduced to 0.63 ± 0.07 (n = 9) compared to the concentration prior to filtration. Thus, the correction of this phenomenon was much more significant for the parent tracer than for the radiometabolites. As the f_P was corrected, the value increased by 59 %.

Because of the low f_P of [^{11}C]SMW139, the radioactivity concentration of the parent tracer in the filtrates was also low, which occasionally led to unanalyzable membrane correction values because of

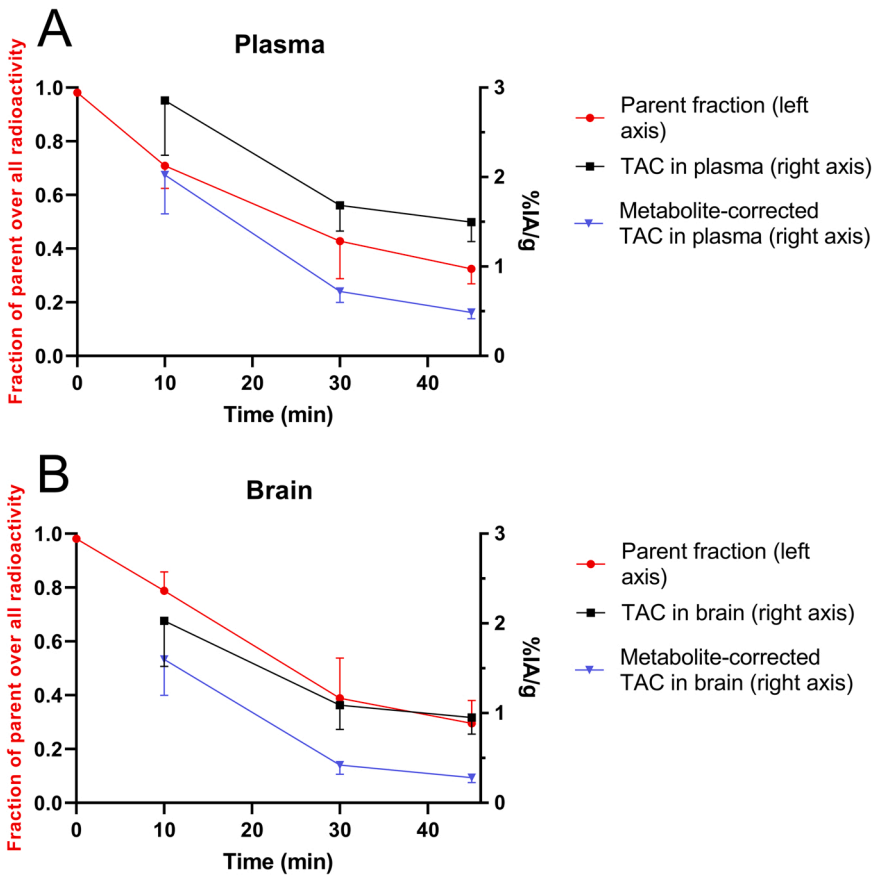

Fig. 4. Parent fraction (red, left y-axis) in plasma (A) and brain (B) as mean and standard deviation of mean. Time-activity curves (TACs, right y-axis) expressing uptake in plasma (A) and brain (B). At the 10-min, 30-min, and 45-min time points, respectively: parent fraction, plasma: n = 19, 14, 13; brain: n = 9, 14, 11; TAC, plasma and brain: n = 45, 14, 7.

insufficient signal-to-noise ratio of the peak corresponding to the parent tracer. In these few cases, we used the mean from the successfully analyzed membrane correction values, which caused only slight inaccuracies because the SD of the membrane filter correction value was minor (Table 1).

3.3.2. f_P and f_M

The f_P was clearly time-dependent (Fig. 5, Table 1). This dependence might have been the result of parent clearance from plasma and freeing of more proteins to bind the remaining analytes at the later time points as the parent-to-protein ratio decreased. Similar explanations have been presented previously [17].

The parent fraction in plasma is presented along with the results for f_P and f_M (Table 1). In addition, the free parent divided by all free radioactivity was calculated to yield the true ratio of parent tracer and radiometabolite concentrations which are free to cross the BBB. The amount of free parent decreased rapidly throughout the studied time points, while the amount of free metabolites remained rather constant (Fig. 6). From 10–45 min, the fraction of free parent relative to all free radioactivity decreased rapidly from 0.085 to 0.019, indicating that most of the protein-free fraction consisted of radiometabolites during these time points. The f_P was low, decreasing from 0.032 to 0.007 from 10 min to 45 min, while f_M remained at much higher levels, between 0.52 and 0.35, during the same time points. A protein-bound fraction acts as a reservoir, stabilizing the concentrations of free analytes [18]. For example, to maintain dynamic equilibrium, part of the parent tracer will be released from the plasma proteins when part of the free parent is diffused out from plasma.

Small size, low molecular weight, un-ionized charge, and low hydrogen bonding potential are other characteristics of a molecule that further favors BBB penetration [19] and should be taken into account, if possible. The radiometabolites of [^{11}C]SMW139 have not been

Table 1
Mean (*M*) and standard deviation of the mean (*SD*) for plasma parent fraction and parent and radiometabolite (metab) free fractions (f_P and f_M). Measured from the same mice. At the 10-min, 30-min, 38-min, and 45-min time points, respectively: n = 3, 4, 2, 4.

	Time point (min)	Plasma parent fraction	f_P, free parent/ all radio- activity	Free parent/ all parent	f_M, free metab/ all radio- activity	Free metab/ all metab	Free parent/ all free radio- activity	Free radio-activity/ all radio- activity
M	10	0.567	0.032	0.057	0.368	0.835	0.085	0.399
SD		0.098	0.000	0.009	0.113	0.119	0.019	0.113
M	30	0.347	0.012	0.034	0.508	0.760	0.023	0.520
SD		0.077	0.005	0.007	0.083	0.092	0.011	0.081
M	38	0.336	0.010	0.031	0.520	0.778	0.019	0.530
SD		0.050	0.001	0.008	0.076	0.056	0.000	0.077
M	45	0.323	0.007	0.021	0.350	0.518	0.019	0.356
SD		0.043	0.002	0.006	0.017	0.035	0.006	0.019

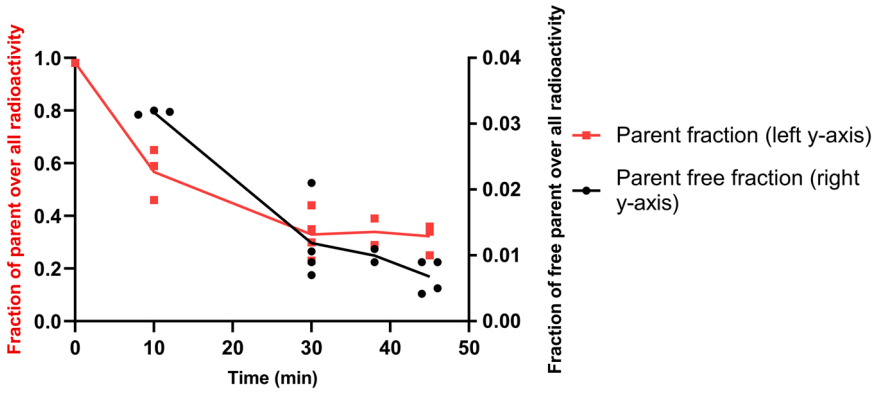

Fig. 5. Parent fraction in plasma (protein-bound + free parent tracer over all ^{11}C-radioactivity in sample, left axis) and free parent fraction, (f_P, free parent over all ^{11}C-radioactivity in sample, right axis) as analyzed from the same mice. Individual values are plotted to show the low variation and correlation of curves. At the 10-min, 30-min, 38-min, and 45-min time points, respectively: n = 3, 4, 2, 4.

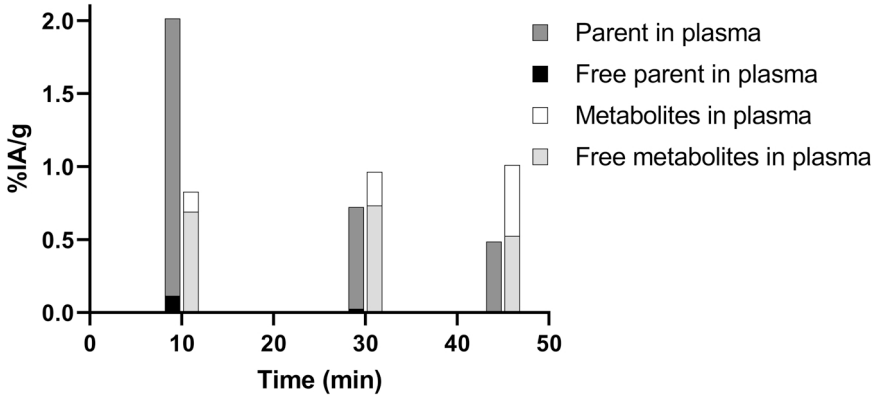

Fig. 6. Total percentage of injected activity/g of plasma (%IA/g) of parent, free parent, total metabolites, and free metabolites in plasma as a time-activity bar chart. %IA/g were analyzed at the 10-min, 30-min, and 45-min time points from n = 45, 14, and 7, respectively. Free fractions were analyzed at the 10-min, 30-min, and 45-min time points from n = 3, 4, and 4, respectively.

identified at the molecular structure level, so we cannot say if the parent tracer is catabolized into smaller molecules or has a larger molecule size and hydrophilicity, for example, because of glucuronidation. In this study, we can only evaluate the lipophilicity (based on the TLC R_f) and free fractions to understand BBB penetration abilities. As the R_f was higher in reversed-phase separation, the radiometabolites were more polar and therefore less lipophilic, so their ability to cross the lipophilic BBB would have been compromised compared to the parent tracer. However, the lipophilicities of the radiometabolites are nevertheless sufficient enough to enable the BBB penetration. The CLogP = 2.90 (Chemdraw Professional 19, PerkinElmer Informatics, Inc.) of [^{11}C]SMW139 is considered to be moderate for crossing the BBB, and the molecular weight of 386.8 g/mol is also acceptable for crossing the BBB [1]. The much higher f_M compared to f_P in plasma at least partly explains why the less lipophilic radiometabolites of [^{11}C]SMW139 accumulate efficiently in the brain.

3.3.3. UF

The Microcon UF device was selected because of the Ultracel low-binding regenerated cellulose membrane and suitability for low-volume samples. A cutoff value of 10 kDa was used, contrary to the 30-kDa cutoff value commonly used in previously published UF methods in protein binding studies [8,20]. The 30-kDa cutoff does not guarantee 100 % protein-free filtrates, as stated in the manufacturer's Membrane Learning Centre, "For example, an UF membrane rated at 30 kDa will exclude a test protein with a molecular weight of 30 kDa. Ninety percent of that test protein will be retained on the upstream side and 10 % will pass through into the filtrate, resulting in concentration of the protein" [21]. Because we are interested in the protein-free filtrate and not the concentrated protein mass in the filter, we reduced the cutoff value to the smallest size generally available to limit possible error sources that could not be properly quantified. The increase in the spinning times was minor with the 10-kDa membrane. One of the main proteins that lipophilic drugs bind to in plasma is albumin (66.5 kDa). Other common proteins in mouse plasma are prealbumin, α1-acid glycoprotein, transferrin, lipoproteins, immunoglobulins, complement proteins, and coagulation proteins [22]. Because we do not know which proteins bind the parent tracer and its radiometabolites, it is rational to keep the cutoff as small as possible.

During UF, the temperature of the sample may slightly affect the equilibrium of the protein binding. The starting temperature here was room temperature, but it generally increases during UF. The optimal situation could be maintaining centrifugation temperature at 36 °C. Also, plasma pH was not adjusted during the study. However, adjustment would have affected the concentrations of the solutions, in turn influencing the delicate equilibrium between the protein-bound and unbound analytes. Our assumption was that introducing such sample preparation steps into the protocol would probably have entailed more harms than improvements to the accuracy of the data. Also, the repeatability could be hampered because it is often difficult to measure and adjust the pH of plasma samples < 100 μL. Toma et al. [23] addressed the effects of such factors recently.

3.3.4. Analyzing free fraction data

To our knowledge, previous studies with [^{11}C]SMW139 or with any other tracer have not analyzed or adequately addressed the importance of the f_M and their part in radioactivity uptake into tissues. Being able to analyze the f_M will increase understanding of the pharmacokinetics of the tracer, which is important when assessing the modeling, usability, and safety of a tracer for new applications. Previous plasma free fraction methods have mostly used plasma samples spiked with high levels of the parent tracer. Such methods are less complex and can use larger radioactivity concentrations. However, *in vitro* methods might not fully represent the delicate dynamic equilibrium present *in vivo*, which also includes free and protein-bound radiometabolites and the parent tracer in low trace-level concentrations. More studies to compare these methods should be performed.

There are several methods to analyze the f_P in drug research. One of the most prevalent has been equilibrium dialysis (ED). ED also has been used for protein binding studies involving PET tracers, but only with *in vitro* samples. The slowness of ED limits its wider use for short-lived PET tracers. Also, ED is not suitable for traditional *in vivo* sample PET studies where the administered tracer amount and especially the amount of radiolabeled free parent tracer and radiometabolites are really low (in the magnitude of pmol/mL in plasma) and the half-life of the radionuclide is short, as with carbon-11 tracers [8,24].

3.3.5. RadioTLC for rapid and simultaneous data collection of many samples at the same time

The time from plasma separation to placing the developed TLC plate with the standard, plasma, brain supernatant, and filtrates into the exposure cassette can be as low as 12 min. Several samples from multiple subjects can be applied to this same plate and analyzed simultaneously, which is a tremendous advantage. Multiple plates also can be developed at the same time. This is a method of choice particularly when short-lived radionuclides are used. The technique developed in this study is rapid and comparable in throughput speed to other fast protein binding analysis techniques, such as high-performance frontal analysis (<12 min per sample) [20].

3.4. Radiometabolite correlation between plasma and brain

The correlation between the percentages of radiometabolites over all radioactivity in plasma and brain correlated significantly (Pearson's, $r = 0.94$), with $R^2 = 0.89$ ($p < 0.001$) and slope = 1.2 (Fig. 7). The percentages of radiometabolites were initially lower in the brain compared to plasma. The percentages of radiometabolites must first rise in the plasma before they can start to accumulate in the brain. The ratio of the radiometabolite fractions rapidly became even between plasma and brain, but with the average slope of 1.2, the fraction of radiometabolites increased faster in the brain than in the plasma. Soon after, the percentages of radiometabolites in the brain exceeded the percentages found in plasma, indicating that the accumulation of radiometabolites through the BBB into the brain was efficient compared to accumulation of the parent tracer in all observed mice and time points. Generally, the metabolites, being less lipophilic, have a poorer ability to cross the BBB. The reason behind the observed correlation can be at least partly explained by the much higher f_M compared to f_P as only the free fraction can diffuse out of the blood vessels into the brain tissue [6].

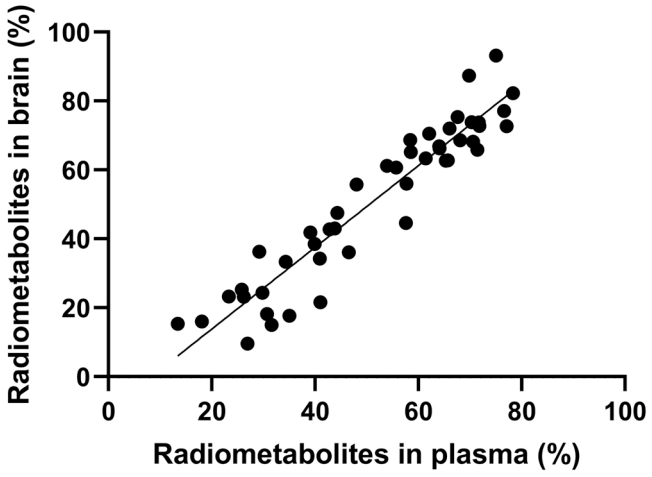

Fig. 7. Correlation plot of percentage of radiometabolites in plasma and brain from mice in which the parent fraction analysis was successfully performed from both plasma and brain (n = 47, including all data from different radioTLC methods (*i.e.*, HPTLC-plate) and all time point mice).

3.5. Radiometabolites crossing the BBB – in vitro mouse brain homogenate study

The chromatographic analyses of the incubated brain homogenate and sham samples showed that they both consisted of > 99 % of parent tracer at all investigated time points. In the chromatogram, the < 1 % of radioactivity that corresponded to R_f regions outside the parent tracer R_f was probably the result of unevenness of the baseline, as the background correction did not remove 100 % of the PSL originating from background radioactivity. Thus, we conclude that radiometabolites are not formed under *in vitro* conditions in brain homogenate, and it is unlikely that they are formed directly in the brain tissue *in vivo*, but rather enter the brain by penetrating the BBB.

3.6. Rationale for the f_P calculating method

As plasma protein binding studies commonly are done with *in vitro* samples [8], the definition for the f_P is the same whether calculating for f_P as free parent over all radioactivity or free parent over all parent radioactivity, because radiometabolites are not considered to be present in *in vitro* samples. When using *in vivo* samples that contain radiometabolites, there are two ways to define f_P. The first is to divide the free parent by all parent (requires analyzing the parent fraction in plasma), and the second is dividing free parent by all radioactivity. The first option can be used for modeling the radioactivity concentration of the free parent when a metabolite-corrected plasma curve is available, and the second can be used if we have just the plasma TAC. It should be noted that the *in vivo* sample containing the free fractions should be analyzed for free parent and free radiometabolite ratio. Hence, with the developed method, we have generated results using both ways to calculate the free fractions to demonstrate their difference (Table 1). The studies that use *in vivo* samples and tracers with significant radiometabolism must define carefully what is being calculated. Is it what is being measured only the free parent, or is it all free radioactivity combined, including the free radiometabolites, divided by the total radioactivity of the sample to yield only the radioactivity-free fraction? Thus, analyzing filtrates by chromatographic methods and the appropriate membrane correction factors from the plasma matrix probably yields results that are more in line with the true values in the plasma.

4. Conclusions

In this study, we introduced a novel method to analyze and calculate the plasma protein binding of a PET tracer, [^{11}C]SMW139, and its radiometabolites to add tools for a more accurate understanding of the pharmacokinetics. The method developed and principles explained here, relying on separate analysis of the f_P and f_M that contribute to the true influx of radioactivity through the BBB into the brain, can be applied for other PET tracers. The approach is especially useful when modeling the behavior of the PET tracers and their radiometabolites in entering the brain. We found that the radiometabolites of [^{11}C]SMW139 have a much larger free fraction than the parent tracer. These

radiometabolites can cross the BBB and are not formed directly in the brain. In addition, a more detailed understanding of f_P and f_M from rodents can be used in translational studies to explain the behavior of the tracer in humans. Similar parent tracer and radiometabolite plasma protein binding methods can be developed for human *in vivo* blood sample analysis.

CRediT authorship contribution statement

Richard Aarnio: Conceptualization, Project administration, Methodology, Validation, Investigation, Writing – original draft, Visualization. **Obada M. Alzghool:** Methodology, Project administration, Investigation, Writing – review & editing. **Saara Wahlroos:** Resources, Formal analysis, Writing – original draft. **James O'Brien-Brown:** Writing – review & editing, Resources. **Michael Kassiou:** Writing – review & editing, Resources. **Olof Solin:** Writing – review & editing, Resources, Funding acquisition. **Juha O. Rinne:** Writing – review & editing, Funding acquisition. **Sarita Forsback:** Supervision, Writing – review & editing. **Merja Haaparanta-Solin:** Supervision, Conceptualization, Investigation, Writing – review & editing, Funding acquisition.

Declaration of Competing Interest

The authors declare that they have no known competing financial interests or personal relationships that could have appeared to influence the work reported in this paper.

Acknowledgements

This study was supported by a grant from state funding for University-level Health Research (project 13250 (MHS), 11133 (OS)), the Swedish Cultural Foundation in Finland (project 178133), and the Academy of Finland (projects 310962 (JOR) and 334310 (OS)).

We thank Marko Vehmanen, Päivi Kotitalo, Aake Honkaniemi, Mira Eisala, and other staff for laboratory technical support in the PET Preclinical Imaging Laboratory, the Central Animal Laboratory of the University of Turku for laboratory animal maintenance, and the staff of the Accelerator Laboratory for radionuclide production. Also, we thank Vesa Oikonen and Francisco López-Picón for valuable comments on the manuscript and Katri Kulmala for image visualization aids.

Appendix A. Supporting information

Supplementary data associated with this article can be found in the online version at doi:10.1016/j.jpba.2022.114860.

References

[1] V.W. Pike, Considerations in the development of reversibly binding PET radioligands for brain imaging, Curr. Med. Chem. 23 (2016) 1818–1869, https://doi.org/10.2174/0929867323666160418114826.
[2] B.K. Lawther, S. Kumar, H. Krovvidi, Blood–brain barrier, Continuing Educat. Anaesth. Crit. Care Pain 11 (2011) 128–132, https://doi.org/10.1093/bjaceaccp/mkr018.
[3] S.S. Zoghbi, K.B. Anderson, K.J. Jenko, D.A. Luckenbaugh, R.B. Innis, V.W. Pike, On quantitative relationships between drug-like compound lipophilicity and plasma free fraction in monkey and human, J. Pharm. Sci. 101 (2012) 1028–1039, https://doi.org/10.1002/jps.22822.
[4] K. Vuignier, J. Schappler, J.-L. Veuthey, P.-A. Carrupt, S. Martel, Drug-protein binding: a critical review of analytical tools, Anal. Bioanal. Chem. 398 (2010) 53–66.
[5] K.K. Ghosh, P. Padmanabhan, C.-T. Yang, S. Mishra, C. Halldin, B. Gulyás, Dealing with PET radiometabolites, EJNMMI Res. 10 (2020) 109.
[6] P.K. Deb, Protein and Tissue Binding: Implication on Pharmacokinetic Parameters, Advances in Pharmaceutical Product Development and Research, Elsevier Inc, 2018, pp. 371–399, https://doi.org/10.1016/B978-0-12-814423-7.00011-3.
[7] C. Wang, N.S. Williams, A mass balance approach for calculation of recovery and binding enables the use of ultrafiltration as a rapid method for measurement of plasma protein binding for even highly lipophilic compounds, J. Pharm. Biomed. Anal. 75 (2013) 112–117.
[8] M.M. Moein, C. Halldin, Sample preparation techniques for protein binding measurement in radiopharmaceutical approaches: a short review, Talanta 219 (2020), https://doi.org/10.1016/j.talanta.2020.121220.
[9] B. Janssen, D.J. Vugts, S.M. Wilkinson, D. Ory, S. Chalon, J.J.M. Hoozemans, R. C. Schuit, W. Beaino, E.J.M. Kooijman, J. van den Hoek, M. Chishty, A. Doméné, A. Van der Perren, A. Villa, A. Maggi, G.T. Molenaar, U. Funke, R.V. Shevchenko, V. Baekelandt, G. Bormans, A.A. Lammertsma, M. Kassiou, A.D. Windhorst, Identification of the allosteric $P2X_7$ receptor antagonist [^{11}C]SMW139 as a PET tracer of microglial activation, Sci. Rep. 8 (2018) 6580, https://doi.org/10.1038/s41598-018-24814-0.
[10] M.H.J. Hagens, S.S.V. Golla, B. Janssen, D.J. Vugts, W. Beaino, A.D. Windhorst, J. O'Brien-Brown, M. Kassiou, R.C. Schuit, L.A. Schwarte, H.E. de Vries, J. Killestein, F. Barkhof, B.N.M. van Berckel, A.A. Lammertsma, The $P2X_7$ receptor tracer [^{11}C]SMW139 as an *in vivo* marker of neuroinflammation in multiple sclerosis: a first-in man study, Eur. J. Nucl. Med. Mol. Imaging 47 (2020) 379–389, https://doi.org/10.1007/s00259-019-04550-x.
[11] M.F. Lister, J. Sharkey, D.A. Sawatzky, J.P. Hodgkiss, D.J. Davidson, A.G. Rossi, K. Finlayson, The role of the purinergic $P2X_7$ receptor in inflammation, J. Inflamm. 4 (2007), https://doi.org/10.1186/1476-9255-4-5.
[12] Q.-H. Zheng, Radioligands targeting purinergic P2X7 receptor, Bioorg. Med. Chem. Lett. 30 (2020), 127169, https://doi.org/10.1016/j.bmcl.2020.127169.
[13] E. Beamer, F. Gölöncsér, G. Horváth, K. Bekő, L. Otrokocsi, B. Koványi, B. Sperlágh, Purinergic mechanisms in neuroinflammation: an update from molecules to behavior, Neuropharmacology 104 (2016) 94–104, https://doi.org/10.1016/j.neuropharm.2015.09.019.
[14] M. Pissarek, Positron emission tomography in the inflamed cerebellum: addressing novel targets among G protein-coupled receptors and immune receptors, Pharmaceutics 12 (2020) 925, https://doi.org/10.3390/pharmaceutics12100925.
[15] M. Haaparanta, T. Grönroos, O. Eskola, J. Bergman, O. Solin, Planar chromatographic analysis and quantification of short-lived radioactive metabolites from microdialysis fractions, J. Chromatogr. A 1108 (2006) 136–139, https://doi.org/10.1016/j.chroma.2005.12.107.
[16] C. Polson, P. Sarkar, B. Incledon, V. Raguvaran, R. Grant, Optimization of protein precipitation based upon effectiveness of protein removal and ionization effect in liquid chromatography–tandem mass spectrometry, J. Chromatogr. B 785 (2003) 263–275, https://doi.org/10.1016/S1570-0232(02)00914-5.
[17] R.L. Nation, U. Theuretzbacher, B.T. Tsuji, Concentration-dependent plasma protein binding: expect the unexpected, Eur. J. Pharm. Sci. 122 (2018) 341–346, https://doi.org/10.1016/j.ejps.2018.07.004.
[18] J.A. Roberts, F. Pea, J. Lipman, The clinical relevance of plasma protein binding changes, Clin. Pharmacokinet. 52 (2013) 1–8, https://doi.org/10.1007/s40262-012-0018-5.
[19] K.E. Warren, Beyond the blood:brain barrier: the importance of central nervous system (CNS) pharmacokinetics for the treatment of CNS tumors, including diffuse intrinsic pontine glioma, Front. Oncol. 8 (2018) 239, https://doi.org/10.3389/fonc.2018.00239.
[20] N. Amini, R. Nakao, M. Shcou, C. Halldin, Determination of plasma protein binding of positron emission tomography radioligands by high-performance frontal analysis, J. Pharm. Biomed. Anal. 98 (2014) 140–143, https://doi.org/10.1016/j.jpba.2014.05.024.
[21] Merck KGaA, Darmstadt, Germany, Membrane Learning Centre, 2021. ⟨https://www.merckmillipore.com/FI/en/life-science-research/chromatography-sample-preparation/membrane-learning-center/Pore-Size-or-NMWL/uyKb.qB.ejgAAAFMYT188eJu,nav⟩. (Accessed 16 November 2021).
[22] Merck KGaA, Darmstadt, Germany, Description of Plasma from Mouse, 2021. ⟨https://www.sigmaaldrich.com/FI/en/product/sigma/p9275?context=product⟩. (Accessed 16 November 2021).
[23] C.-M. Toma, S. Imre, C.-E. Vari, D.-L. Muntean, A. Tero-Vescan, Ultrafiltration method for plasma protein binding studies and its limitations, Processes 9 (2021) 382, https://doi.org/10.3390/pr9020382.
[24] R.N. Gunn, S.G. Summerfield, C.A. Salinas, K.D. Read, Q. Guo, G.E. Searle, C. A. Parker, P. Jeffrey, M. Laruelle, Combining PET biodistribution and equilibrium dialysis assays to assess the free brain concentration and BBB transport of CNS drugs, J. Cereb. Blood Flow Metab. 32 (2012) 874–883, https://doi.org/10.1038/jcbfm.2012.1.